Cellular and Molecular Bioengineering, Vol. 15, No. 6, December 2022 *(© 2022)* pp. 553–569
https://doi.org/10.1007/s12195-022-00745-9

Original Article

Role of Lymphatic Endothelium in Vascular Escape of Engineered Human Breast Microtumors

Alex J. Seibel,[1] Owen M. Kelly,[1] Yoseph W. Dance,[1] Celeste M. Nelson,[2,3] and Joe Tien [1,4]

[1]Department of Biomedical Engineering, Boston University, 44 Cummington Mall, Boston, MA 02215, USA; [2]Department of Chemical and Biological Engineering, Princeton University, 303 Hoyt Laboratory, 25 William Street, Princeton, NJ 08544, USA; [3]Department of Molecular Biology, Princeton University, Princeton, NJ, USA; and [4]Division of Materials Science and Engineering, Boston University, Boston, MA, USA

(Received 21 June 2022; accepted 6 October 2022; published online 7 November 2022)

Associate Editor Michael R. King oversaw the review of this article.

Abstract

Introduction—Lymphatic vasculature provides a route for metastasis to secondary sites in the body. The role of the lymphatic endothelium in mediating the entry of breast cancer cells into the vasculature remains unclear.

Methods—In this study, we formed aggregates of MDA-MB-231 human breast carcinoma cells next to human microvascular lymphatic endothelial cell (LEC)-lined cavities in type I collagen gels to model breast microtumors and lymphatic vessels, respectively. We tracked invasion and escape of breast microtumors into engineered lymphatics or empty cavities under matched flow rates for up to sixteen days.

Results—After coming into contact with a lymphatic vessel, tumor cells escape by moving between the endothelium and the collagen wall, between endothelial cells, and/or into the endothelial lumen. Over time, tumor cells replace the LECs within the vessel wall and create regions devoid of endothelium. The presence of lymphatic endothelium slows breast tumor invasion and escape, and addition of LEC-conditioned medium to tumors is sufficient to reproduce nearly all of these inhibitory effects.

Conclusions—This work sheds light on the interactions between breast cancer cells and lymphatic endothelium during vascular escape and reveals an inhibitory role for the lymphatic endothelium in breast tumor invasion and escape.

Keywords—Triple-negative breast cancer, Lymphovascular invasion, Intravasation, Mosaic vessel, Microphysiological system, Microvascular tissue engineering, Tumor engineering.

Address correspondence to Celeste M. Nelson, Department of Chemical and Biological Engineering, Princeton University, 303 Hoyt Laboratory, 25 William Street, Princeton, NJ 08544, USA; Joe Tien, Department of Biomedical Engineering, Boston University, 44 Cummington Mall, Boston, MA 02215, USA. Electronic mails: celesten@princeton.edu, jtien@bu.edu

ABBREVIATIONS

CM	Conditioned medium
LEC	Lymphatic endothelial cell
LM	Lymphatic medium
LVI	Lymphovascular invasion
TM	Tumor medium

INTRODUCTION

Metastasis is the main cause of cancer-related death in breast cancer patients.[54] Cancer cells must migrate to, escape into, and disseminate through the vasculature before they can reach a secondary site.[44] The lymphatic vasculature is essential to lymph node metastasis and has gained attention as a potential path for distant metastatic spread.[21,32] Although metastatic spread can occur through the blood or lymphatic vasculature, lymphatic vessels offer less resistance to intravasation than blood vessels do: to enter blood vessels, cancer cells must breach the basement membrane, which initial lymphatics lack.[40] Initial lymphatics are also leakier than blood vessels and lack perivascular cells.[6] In tissue sections from human breast cancer patients, tumor cell clusters are found more frequently within lymphatic vessels than within blood vessels.[29] The initial movement of breast cancer cells into lymphatic vessels remains a crucial, but underinvestigated, step in breast cancer metastasis.

Recent studies suggest that the lymphatic vasculature can directly or indirectly contribute to distant metastatic spread of breast cancer cells. Lymphangiogenesis and increased lymphatic density provide

greater surface area for tumor cells to enter the lymphatic vasculature and are associated with worse patient prognosis.[56,57] The presence of tumor cells within neighboring lymphatic vessels of primary breast tumors is associated with both regional and distant metastases.[29–31] Lymph nodes are often the first sites of metastatic spread, and lymph node involvement is one of the strongest predictors of poor prognosis in breast cancer.[4,20] In mice, breast cancer cells can enter the bloodstream at lymph nodes to seed distant metastases.[35]

Crosstalk between tumor cells and lymphatic endothelial cells (LECs) can promote tumor advancement toward and entry into the lymphatic vasculature. Cancer cells induce lymphangiogenesis by secreting a variety of growth factors, including vascular endothelial growth factor-C/D (VEGF-C/D), angiopoietins, platelet-derived growth factor, and basic fibroblast growth factor.[40] Tumor cell-derived eicosanoids increase adhesion of tumor cells to endothelium and cause LEC retraction, both of which can facilitate transendothelial migration of tumor cells.[23,50] Conversely, LECs can induce the proliferation, directional invasion, and transendothelial migration of breast cancer cells. Tumor-educated LECs secrete more epidermal growth factor (EGF) than naïve LECs do, which enhances the proliferation of MDA-MB-231 triple-negative human breast cancer cells.[25] Expression of CCL21 by LECs can promote transmigration of tumor cells across lymphatic endothelium.[37] CCL21-mediated signaling is also linked to lymph node metastasis of human breast cancer.[7]

The study of tumor cells entering vasculature *in vivo* is typically limited to indirect measures long after intravasation has occurred, such as counts of circulating tumor cells or distant metastases. Intravital microscopy can be used to visualize intravasation more directly.[22,55] This approach has revealed tumor cells shedding into lymphatic vessels and transporting *via* lymph flow in real time.[9,17] Although a powerful technique, intravital microscopy of lymphatics requires fluorescent tracers to be injected into the peritumoral tissue, which limits image resolution and contrast.

In principle, *in vitro* models offer more geometric control, are more reproducible, and are easier to image than *in vivo* models are.[15] A Transwell model has been used to study transendothelial migration of MDA-MB-231 cells across lymphatic endothelium, but the LECs in this model lack the 3D geometry of lymphatic vessels *in vivo*.[37] Other studies have co-cultured breast (and other) cancer cells next to engineered blood microvessels and have observed a variety of mechanisms by which tumor cells can overtake and/or gain entry into vessels, including intravasation, endothelial ablation, and the formation of mosaic vessels.[34,43,52] Our previous work has studied the invasion and escape of engineered breast microtumors into adjacent empty blind-ended cavities, with the cavities serving as an "artificial lymphatic." These studies have revealed how interstitial fluid pressure, matrix pore size, matrix metalloproteinase activity, proliferation, and adipose stroma affect breast cancer cell invasion and escape.[11,39,46,47]

In the current study, we extend the microtumor model to include lymphatic microvessels, i.e., blind-ended cavities lined by lymphatic endothelium. We then use this tumor-lymphatic model to characterize how tumor cells escape into/along lymphatic vessels and elucidate how the lymphatic endothelium affects breast cancer cell escape. We demonstrate that escaped tumor cells can present either between the endothelium and the surrounding collagen wall, in line with the endothelium, or within the endothelial lumen. Several days after initial escape, portions of the endothelial lining at the tip of the vessel can collapse or delaminate and be replaced by a growing mass of escaped tumor cells. We compared tumor invasion and escape into empty cavities and lymphatic vessels under matched average flow rates and found that the presence of the lymphatic endothelium slows the invasion of breast tumors toward the cavity and delays escape into the cavity. By itself, exposure to LEC-conditioned medium is sufficient to slow the escape of tumor cells into empty cavities, which suggests an inhibitory role of LEC-derived factors. Moreover, lymphatic endothelium delayed the escape of tumor cells once they reached the vessel, an effect that was not observed in tumors treated with LEC-conditioned medium alone in an endothelium-free condition, which suggests that the lymphatic endothelium also plays a physical role in inhibiting escape.

MATERIALS AND METHODS

Cell Culture

GFP-expressing MDA-MB-231 human breast carcinoma cells (Angio-Proteomie) were cultured in tumor medium (TM), which consisted of DMEM:F12 (Hyclone) supplemented with 10% heat-inactivated fetal bovine serum (FBS, lot #B18020; Atlanta Biologicals) and 50 μg/mL gentamicin (Sigma). Tumor cells were routinely cultured at 37 °C under 5% CO_2 and passaged using 0.005% trypsin (Invitrogen) every 3–4 days at a 1:6 to 1:8 ratio through passage fifteen.

Human dermal lymphatic microvascular endothelial cells (LECs, lots #0070602 and #2011204 from male donors, ages 3 and 4, respectively; Promocell) were cultured on gelatin-coated tissue culture plates in

lymphatic culture medium (LM), which consisted of MCDB131 (Caisson) supplemented with 10% FBS, 1% glutamine-penicillin–streptomycin (Invitrogen), 1 μg/mL hydrocortisone (Sigma), 80 μM dibutyryl cyclic AMP (db-cAMP; Sigma), 25 μg/mL endothelial cell growth supplement (Alfa Aesar), 2 U/mL heparin (Sigma), and 0.2 mM ascorbic acid 2-phosphate (Sigma). LECs were passaged using 0.005% trypsin every 3–4 days at a 1:4 to 1:10 ratio through passage nine.

Formation of Engineered Microtumors and Lymphatic Vessels

Breast microtumors with and without lymphatic vessels (n = 93 and 97, respectively) were formed by adopting a needle-based approach to mold cavities in type I collagen gels (Fig. 1).[47] Briefly, chambers of polydimethylsiloxane (PDMS) were UV/ozone-treated and placed onto glass coverslips. The interior channels of the chambers were then coated with poly-D-lysine (300 kDa, 1 mg/mL in PBS; Sigma). Two acupuncture needles (120-μm-diameter; Seirin) were coated with bovine serum albumin (BSA, 1% in PBS; Calbiochem) and aligned end-to-end from opposite sides of each PDMS chamber. Prior to treatment with BSA, needles for empty cavities and lymphatic vessels were rounded by gently brushing the tops of the needles over a benchtop. Bovine dermal type I collagen (4.9 mg/mL, acid-extracted, lot #210090; Koken) was mixed on ice with 0.2 M NaOH, 10× Hanks' balanced salt solution (Gibco), DI water, and TM to a final collagen concentration of 3.9 mg/mL, a final FBS concentration of 0.4%, and a pH of 9–9.5. Neutralized collagen was added to the chambers and gelled at 37 °C for 25 min before hydrating with LM. Gels were incubated for at least another 35 min at 37 °C before removing the needles, yielding two opposing blind-ended cavities 100–200 μm apart in the middle of the gel.

The rounded cavity was either lined with LECs or left unseeded. To seed LECs into the cavity, we added ~ 5 μL of a dense LEC suspension (~ 10^7 cells/mL in LM) to the well adjacent to the open end of the cavity under slight hydrostatic pressure. After cells flowed into the cavity and reached its tip, the dish was tilted to flush any non-adherent cells out of the cavity and to prevent additional cells from entering the cavity. Fifteen minutes later, LM (~ 50 μL) was added to the opposite well to flush any remaining non-adherent cells out of the seeded cavity. In some cases, LECs were labeled with red PKH26 dye (10 μL/mL in Diluent C; Sigma) one day before seeding. Immediately after seeding LECs, a suspension of MDA-MB-231 cells (~ 70 μL, 1–2 × 10^6 cells/mL in LM) was introduced into the tumor well, creating a > 600-μm-long, densely-packed "microtumor" inside the cavity opposite the LEC-seeded one. The day of seeding is considered day 0.

After sequentially seeding LECs and tumor cells, we switched the sample medium to a stabilizing medium (LM+), which consisted of LM supplemented with 400 μM db-cAMP (final concentration), 20 μM phosphodiesterase inhibitor Ro-20–1724 (Calbiochem), and 3% 60–90 kDa dextran (MP Biomedicals); these additives promote vessel stability.[26,53] For the first two days after seeding, we refed samples by adding 70 μL LM+ to the tumor well and 60 μL LM+ to the opposite (lymphatic or empty cavity) well. Two days post-seeding (i.e., on day 2), PDMS spacers were added to the wells adjacent to the empty cavity or lymphatic vessel and filled with medium to generate hydrostatic pressure and flow toward the tumor well (~ 2.5 μL/h). To obtain the desired flow rate, we used a pressure head of ~ 0.6 cm H_2O for samples with empty cavities adjacent to the tumors. To maintain similar flow rates in lymphatic vessels as the endothelial barrier strengthened, we increased pressures up to ~ 1.8 cm H_2O over the first two days of flow by adding extra PDMS spacers and medium to the lymphatic well. Flow rates were monitored by measuring the volume of medium that accumulated in the tumor well over 12–16 h and reported as the average flow rate after adjusting for evaporation. Evaporation rate was found by adding 50 μL of medium to each well of a control sample in the absence of flow and measuring the volume loss over time. Once flow rates stabilized (~ 2 days after the start of flow for lymphatic samples), samples were refed twice daily until sixteen days post-seeding by adding fresh medium (25–50 μL LM+) to the upstream well of each sample and removing all medium from the downstream well.

Lymphatic samples were discarded if the endothelium did not reach confluence by day 3 after seeding or if the maximum applied pressure (1.8 cm H_2O) was insufficient to obtain a flow rate of 2.5 μL/h. In some lymphatic samples, the collagen gel detached from the PDMS chamber over time. These samples were censored when detachment of the gel caused the vessel to deform within 500 μm of the vessel tip and/or escaped cancer cells.

Assessment of Tumor Invasion, Escape, and Spread

Phase-contrast and fluorescence images were acquired daily using an Axiovert 200 inverted microscope (Zeiss), 10×/0.30 *NA* Plan-Neofluar objective, and Axiocam MRm camera (Zeiss) at 1040 × 1388 resolution. Three-dimensional tumor-cavity distances (D) were found by measuring the smallest 2D in-plane distance from the tumor to the cavity, measuring the difference in focal plane height between the tumor and cavity, and calculating the Euclidean distance. The difference in focal

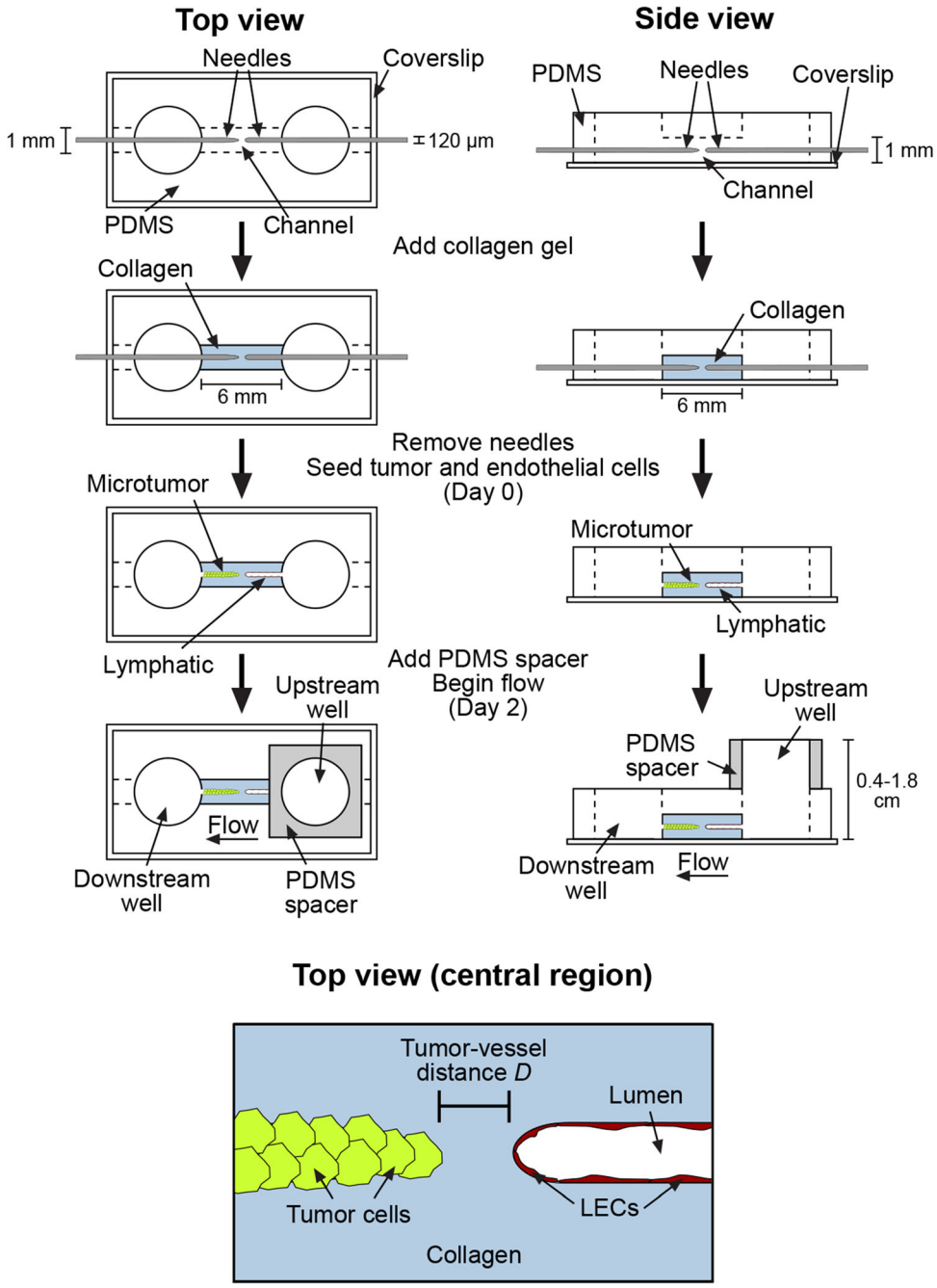

FIGURE 1. Schematic of the procedure to form 3D breast microtumors next to lymphatic vessels. Opposing blind-ended cavities were molded in collagen gels and seeded with tumor cells and LECs to form a solid tumor and a lymphatic vessel with an open lumen, respectively. To form tumors next to empty cavities, we did not seed LECs into the cavity opposite the tumor. After two days, flow was established so that the lymphatic or cavity was upstream of the tumor.

plane height was multiplied by a factor of 1.358 to correct for the index of refraction of culture medium.[49] Tumor-cavity distances were measured daily. Speed of tumor invasion toward the cavity was calculated using tumor-cavity distance data from day 2 until day 8 or the day of escape, whichever was earlier. A tumor was considered to have invaded when at least one cell body within 500 μm from the tip of the tumor was observed to be located at least 20 μm from the initial boundary of the tumor. A tumor was considered to have escaped when at least one entire cancer cell body (spread or rounded) was observed within the blind-ended cavity opposite the tumor. For lymphatic samples, "escaped" cancer cells consisted of cells that had intravasated across the endothelium, cells that had spread along the wall of the cavity between the collagen and the endothelial layer, and cells that had

migrated into a region that was devoid of endothelial cells. A 63×/0.95 *NA* Achroplan water immersion objective was used to confirm whether an escaped, circular GFP-expressing tumor cell or cluster of tumor cells was inside the endothelial lumen. We could not always conclusively determine whether tumor cells that had spread at the vessel wall were on the apical or basal side of the endothelium.

Tumor diameter was measured as the maximum radial thickness of the tumor in the phase-contrast images. Escape delay was assessed by measuring the time between when a tumor cell body first contacted/overlapped the empty cavity or lymphatic vessel (i.e., when $D = 0$ μm) and the time of escape (i.e., when the entire tumor cell was within the cavity). Speed of post-escape tumor spread was quantified by tracking the location of the furthest escaped cancer cell along the cavity, on each day from the initial day of escape until the end of the experiment. This metric did not distinguish between tumor cells that migrated between the endothelium and collagen wall, in regions without LECs, or within the vessel lumen.

Measurement of Collagen Permeability

Unpatterned 1 mm × 1 mm × 6 mm collagen gels were formed in PDMS chambers. Gels were placed under a hydrostatic pressure difference of ~ 1.4 cm H_2O using PDMS spacers filled with TM, and medium that flowed downstream was collected after 2–2.5 h. Darcy permeability (k) was calculated using the equation $k = Q\mu L/A\Delta P$ where Q is the volumetric flow rate, μ is the viscosity of culture medium (0.72 cPoise at 37 °C), L is the length of the gel, A is the cross-sectional area of the gel, and ΔP is the hydrostatic pressure difference. Darcy permeability of these gels was measured to be 0.067 ± 0.009 μm^2 (mean ± SD).

Collection of Conditioned Medium

LEC-conditioned medium was obtained by culturing LECs to confluence in 60-mm-diameter tissue culture dishes, feeding the confluent LECs with LM+ (5 mL/dish) for two days at 37 °C, collecting the medium, and freezing the medium at − 80 °C until future use. Control medium was obtained by adding LM+ to empty dishes for two days at 37 °C before collecting and freezing. Medium was thawed and sterile-filtered (0.2 μm; Corning) before use.

Immunofluorescence and EdU Staining

Tumors engineered with or without vessels were fixed and stained as described previously.[36] Samples were fixed in 4% paraformaldehyde (PF; Electron Microscopy Sciences) for 15 min at room temperature. After fixation, samples were excised along with the PDMS chambers from the underlying coverslip with a razor blade, gently removed from the PDMS chambers with tweezers, and placed into 1.7 mL microcentrifuge tubes for the remaining steps. Samples were permeabilized with a solution of 0.2% Triton X-100 (Sigma) in PBS (i.e., PBST) for 30 min and were treated for 4 h at room temperature with a blocking buffer that consisted of 5% goat serum (GS; Invitrogen) in PBST. Primary antibodies were prepared in blocking buffer, applied overnight at 4 °C, and removed with PBST for 3–4 h at room temperature. An identical method was used to apply secondary antibodies and Hoechst 33342 (1 μg/mL; Invitrogen). Primary antibodies and working concentrations were mouse anti-cytokeratin (clone AE-1/AE-3, 5 μg/mL; Novus Biologicals), mouse anti-vimentin (clone V9, 8.7 μg/mL; Sigma), mouse anti-PECAM-1 (clone WM-59, 10 μg/mL; Sigma), rabbit anti-Prox1 (1:1000, absolute concentration unknown; Upstate), and mouse anti-VE-cadherin (clone 75, 2.5 μg/mL; BD Transduction Laboratories). Primary antibodies were replaced with mouse IgG (Sigma) at matching concentrations to detect background staining. Highly cross-adsorbed Alexa Fluor 594-conjugated goat anti-mouse IgG and anti-rabbit IgG (5 μg/mL; Invitrogen) were used as secondary antibodies.

An IgG control was not used for Prox1 stains since the concentration for the Prox1 antibody was unknown. Instead, LECs or tumor cells were seeded on coverslips and cultured to confluence for positive and negative controls, respectively. Cells were fixed in 4% PF in PBS for 10 min at room temperature and treated with blocking buffer for 1 h at room temperature. Primary antibody was added to the coverslips overnight at 4 °C. Samples were washed with PBST three times for 20 min each. Secondary antibody was applied for 1 h at room temperature, and coverslips were again washed with PBST three times for 20 min each.

Proliferating cells were visualized using the Click-iT EdU Alexa Fluor 594 Kit (Thermo Fisher Scientific). On day 7, samples were switched for 2 h to medium that contained 20 μM EdU and subsequently fixed with 4% PF in PBS for 15 min at room temperature. Samples were then transferred from chambers to microcentrifuge tubes and stained according to the manufacturer's protocol.

Assessment of Tumor Ablation of Endothelium

Escaped tumor-lymphatic samples were fixed and stained for PECAM-1 as described above. Samples were imaged at the midplane of the vessels. Heatmaps of ablation were generated at single-pixel resolution in a manner similar to one previously described.[26] PE-

CAM-1 signal was used to assess the coverage of lymphatic endothelium on the collagen wall. GFP signal was used to assess the coverage of tumor cells on the collagen or vessel wall. Separate binary arrays were produced for the upper and lower profiles at the mid-plane of each vessel for both endothelial and tumor cell coverage. We defined "ablated region length" as the distance from the cavity tip to the first LEC on the cavity border and "transition region length" as the distance from the end of the ablated region to the escaped tumor cell furthest from the tip of the cavity. Ablation and transition region lengths were measured for both the upper and lower profiles of each vessel and averaged for each sample. MATLAB was used to generate colormaps of endothelial and tumor cell coverage averaged over all samples.

Histological Analysis of Escaped Tumor-Lymphatic Samples

Escaped tumor-lymphatic samples that had been stained for PECAM-1 were further used to obtain cross-sectional images of the lymphatic vessels. A 2% agarose solution was prepared by dissolving agarose (Bio-Rad Laboratories) in Milli-Q H_2O in a microwave and cooling the solution to 45 °C. Samples were submerged in agarose solution for 15 min at 45 °C, placed on ice for 1 h to solidify the agarose, and stored at 4 °C until further use. Cross-sections were obtained by reorienting samples, embedding them in a second 2% agarose gel, and cutting 200-μm-thick sections on a Compresstome VF-310-0Z (Precisionary) following the manufacturer's protocol. Immunofluorescence images were acquired using a 63×/0.95 *NA* Achroplan water immersion objective.

Statistics

Statistical tests were conducted using Graphpad Prism ver. 5. Kaplan–Meier curves were compared using the log-rank (Mantel-Cox) test. Measurements of 3D tumor-cavity distance, tumor bulk diameter, and flow rate were compared using two-way repeated measures ANOVA. Statistical comparisons for tumor-cavity distances only considered distances from day 2 to day 8. Tumor speed to cavity, escape delay, and speed of post-escape spread were compared using Mann–Whitney *U* tests. Tumor ablation metrics were compared using a Spearman correlation test. A p value of less than 0.05 was considered statistically significant. Continuous data are provided as mean ± SD.

RESULTS

Characterization of Engineered Microtumors Adjacent to Lymphatic Vessels

To study how lymphatic endothelium affects breast cancer cell invasion and escape, we formed aggregates of MDA-MB-231 cells adjacent to LEC-lined cavities within collagen matrices (Fig. 2A-B). The tumor cells constitutively expressed GFP, which facilitated tracking of tumor cells as they invaded toward and escaped into adjacent cavities. Although intravasation is the most common route by which tumor cells disseminate into lymphatics, other routes of lymphatic-associated spread have been reported[10,27]; we thus chose a broader definition of "escape" that includes these possibilities. This definition of escape only requires that an entire tumor cell body lies within the walls of the adjacent cavity. For example, tumor cells between the collagen wall and the endothelial layer, in regions

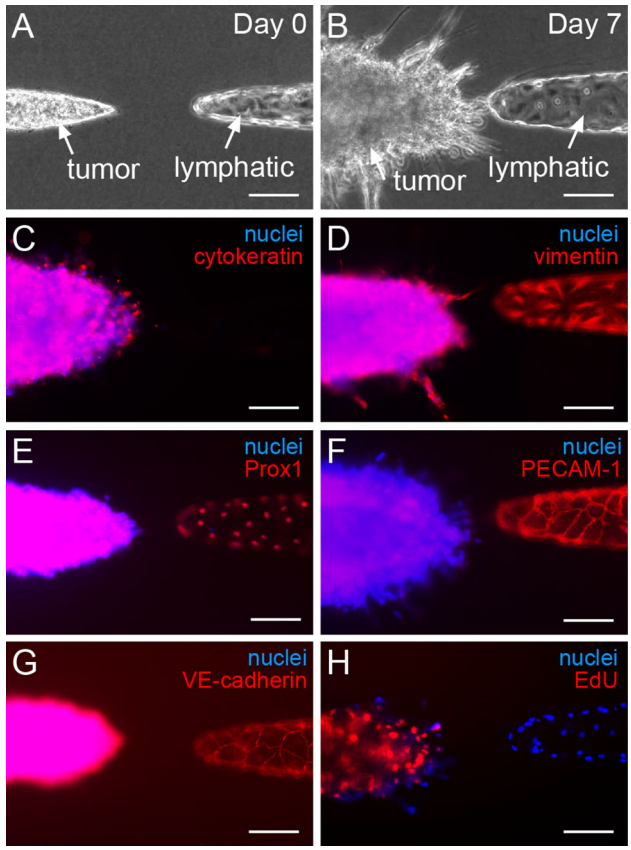

FIGURE 2. Characterization of the engineered tumor-lymphatic model. (A-B) Phase-contrast images at day 0 (A) and day 7 (B) of a microtumor adjacent to a lymphatic vessel. (C-G) Immunofluorescence images of engineered tumors and lymphatic vessels stained for (C) cytokeratin, (D) vimentin, (E) Prox1, (F) PECAM-1, and (G) VE-cadherin. (H) EdU incorporation analysis to visualize proliferating cancer cells and LECs. Scale bars indicate 100 μm. Images in (C)-(H) were obtained from samples on day 7.

devoid of endothelial cells, or inside the lumen of the lymphatic are all considered to have escaped.

We first used immunofluorescence analysis to characterize the model on day 7. To account for background staining, we compared all stains to negative controls at matched exposure times (Fig. S1). We observed a moderate cytokeratin signal (Fig. 2C, compared to Fig. S1A) and strong vimentin signal (Fig. 2D, compared to Fig. S1B) within the microtumors, consistent with the mesenchymal phenotype of triple-negative, basal-like MDA-MB-231 cells. As expected, LECs also stained positively for vimentin.[16] We further characterized the model by staining for endothelial markers. LECs stained positively for the LEC-specific transcription factor Prox1 (Fig. 2E) and showed continuous PECAM-1 (Fig. 2F) and VE-cadherin (Fig. 2G) signal at endothelial junctions. Continuous junctions are expected under the stabilizing culture conditions used in this study.[38] The PECAM-1 and VE-cadherin signals within the microtumors were similar to or below that of IgG negative controls (Fig. S1C-D). As a negative control, Prox1 signal was not present in tumor cells on coverslips (Fig. S1E). Tumor cells actively proliferated (~ 15% EdU^+ along tumor boundary within 600 μm of tumor tip), whereas LECs rarely did (~ 1% EdU^+ within 600 μm of vessel tip) (Fig. 2H). Taken together, the engineered tumor-lymphatic samples demonstrate several key characteristics of human breast tumors and lymphatic vessels.

Location of Escaped Tumor Cells Relative to Lymphatics

To study how breast cancer cells escape into lymphatic vessels, we engineered breast microtumors adjacent to lymphatic vessels and monitored them daily for up to sixteen days (Fig. 3A). Invasions consistently emerged approximately one day after introduction of flow, and were predominantly comprised of multicellular collectives rather than of single cells. In some samples, we observed a delay between when a tumor cell made contact with the abluminal side of the lymphatic endothelium ($D = 0$ μm) and when the tumor cell escaped into the cavity. We define the time of escape as the first moment when an entire cancer cell exits the collagen matrix and enters wholly within the boundary of the cavity. Escape typically presented first as a tumor cell spreading along the wall of the vessel, although we could not definitively determine from daily images whether the escaped cells were located between the endothelium and the collagen wall (i.e., extravascular), in line with the endothelium, or within the lumen (i.e., intravascular). In some samples, we observed rounded, intravascular tumor cells or cell clusters, including at locations near where escaped cells had been present on the vessel wall the previous day (Fig. 3B). We observed intravascular cells move and/or disappear as time progressed. Within five days of initial escape, we observed at least one rounded, intravascular tumor cell (either singly or as a cluster) in ~ 50% of samples. Although it is tempting to interpret these rounded intraluminal cells as evidence of local intravasation, we cannot exclude the possibility that these cells originated through some other means (e.g., tumor cells replacing the endothelium and later detaching and/or proliferating).

To better visualize the location of escaped tumor cells relative to the endothelium in this system, we stained tumor-lymphatic samples for PECAM-1, both in intact samples and in agarose-embedded cross-sections. We observed escaped tumor cells in different positions relative to the lymphatic endothelium: 1) extravascular, 2) in line with the endothelium, and 3) intravascular (Fig. 4A). Cross-sections of tumor-lymphatic samples revealed similar locations of escaped tumor cells as observed from side views of the vessel midplanes (Fig. 4B). Escaped tumor cells that were located outside (extravascular) or in line with the endothelium predominantly exhibited a spread morphology, whereas those that were located inside the endothelium (intravascular) had a rounded morphology. It is possible that intravascular tumor cells adhered to either the luminal side of the endothelium and/or to other tumor cells. Sections far from the tip of the vessel were devoid of tumor cells and showed a thin continuous ring of PECAM-1 signal (Fig. 4C).

Several days after escape occurred, the endothelium was often delaminated from or missing from the vessel tips as tumor cells filled the space along the cavity wall. A previous study referred to this process as endothelial "ablation".[34] Using side views of samples stained for PECAM-1 on day 16, we analyzed the coverage of endothelial and tumor cells along the upper and lower vessel walls and created binary coverage maps at single-pixel resolution from images of the midplane of the vessel (Fig. 5A). We used the absence of PECAM-1 signal to define where the lymphatic endothelium was absent or delaminated from the cavity wall, and the presence of GFP signal to define the location of tumor cells along the cavity wall. An averaged heatmap was generated for both endothelial and tumor cell coverage (Fig. 5B), revealing greater tumor cell coverage ($p < 0.0001$, $r = -0.99$) and endothelial delamination ($p < 0.0001$, $r = 0.96$) at the vessel tip compared to more distal regions of the vessel.

We partitioned images of vessels of escaped microtumors, starting from the tip of the vessel, into three contiguous regions: 1) an "ablated region" where tumor cells have completely replaced endothelial cells (i.e., LECs are no longer present) along the cavity

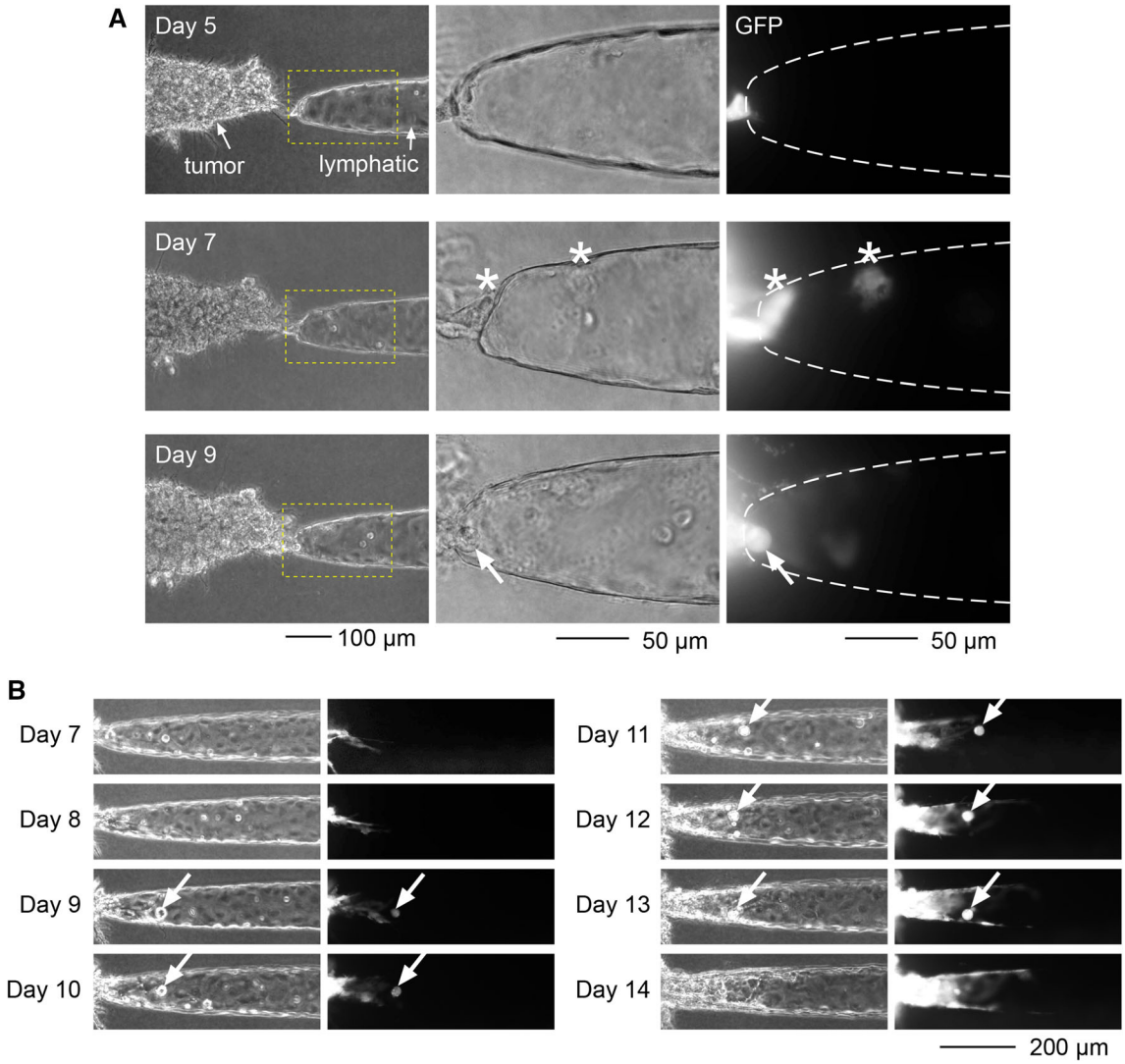

FIGURE 3. Progression of escape of tumor cells relative to lymphatic vessels. (A) Time-lapse images of breast cancer cell escape. Shown are phase-contrast (*left, middle*) and fluorescence (*right*) images of a tumor-lymphatic sample. Images of the dashed regions (*middle, right*) are taken at 63× magnification. Asterisks indicate escaped cancer cells. Arrows indicate intravascular cancer cells. (B) Time-lapse images recording the behavior of a cluster of intravascular tumor cells. Arrows indicate the location of a cluster of tumor cells.

border, 2) a "transition region" where a mixture of tumor cells and endothelial cells occupy the cavity border, and 3) an "intact region" comprised of endothelium devoid of tumor cells (Fig. 5A). The lengths of the ablated regions for the top and bottom borders were averaged for each sample, and similarly for the transition regions. The lengths of the ablated region ($p = 0.0005$, $r = 0.63$; Fig. 5C) and transition region ($p = 0.023$, $r = 0.44$; Fig. 5D) both increase with time after escape, which implies a sequence of tumor cell escape, migration, and ablation.

The Presence of a Lymphatic Endothelium Slows Escape of Breast Microtumors

To define how the lymphatic endothelium affects the kinetics of breast cancer invasion and escape, we cultured breast microtumors next to empty cavities or lymphatic vessels (Fig. 6A) and monitored them for sixteen days with matched starting tumor-cavity/tumor-lymphatic distances (Fig. S2A) and average flow rates (2.41 ± 0.55 μL/h for empty cavities, 2.50 ± 0.74 μL/h for lymphatic vessels, $p = 0.52$; Fig. S2B). Matching flow rates required the use of higher driving

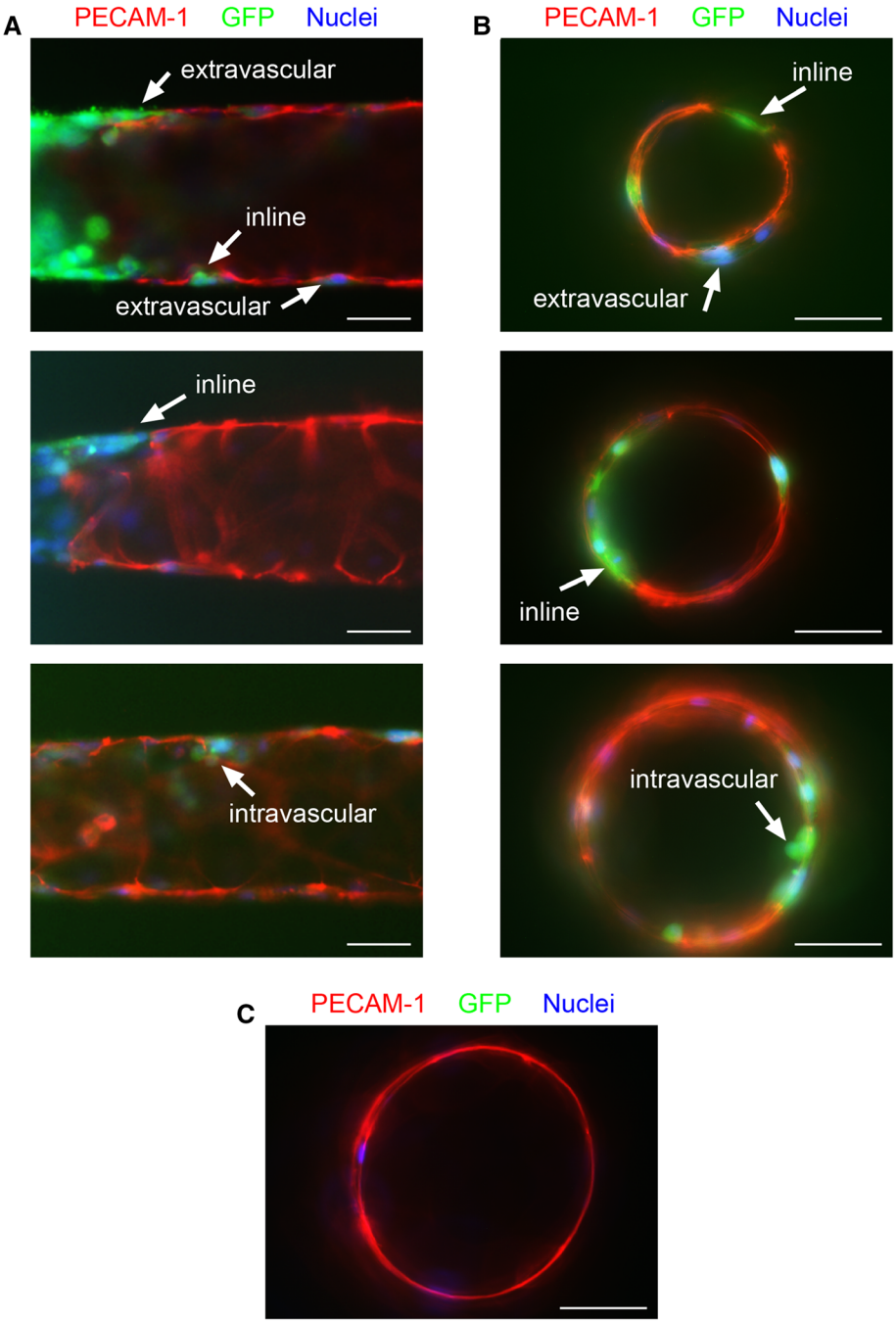

FIGURE 4. Location of escaped tumor cells relative to lymphatic vessels. (A) Side views of escaped tumor-lymphatic samples with extravascular, inline, and/or intravascular tumor cells. (B) Cross-sectional views of escaped tumor-lymphatic samples with extravascular, inline, and/or intravascular tumor cells. (C) Cross-sectional view of endothelium-only region of escaped tumor-lymphatic sample. Scale bars indicate 50 μm. Images in (B) and (C) were taken at 63× magnification.

pressures in tumor-lymphatic samples to overcome the hydraulic resistance imposed by the LEC monolayer (Fig. S2C). The lymphatic endothelium did not affect the kinetics of tumor invasion ($p = 0.29$; Fig. 6B). Surprisingly, the lymphatic endothelium delayed the escape of tumor cells ($p < 0.0001$; hazard ratio (HR) 7.4; 95% confidence interval (CI), 4.1–13.2; Fig. 6C).

To uncover how lymphatic endothelium slows escape, we measured other metrics of tumor progression including tumor growth rate, tumor speed toward the adjacent cavity, delay before escape, and the speed of post-escape spread along the cavity. Tumor growth was assessed by measuring the radial thickness of the tumor bulk over time. Microtumors that were adjacent

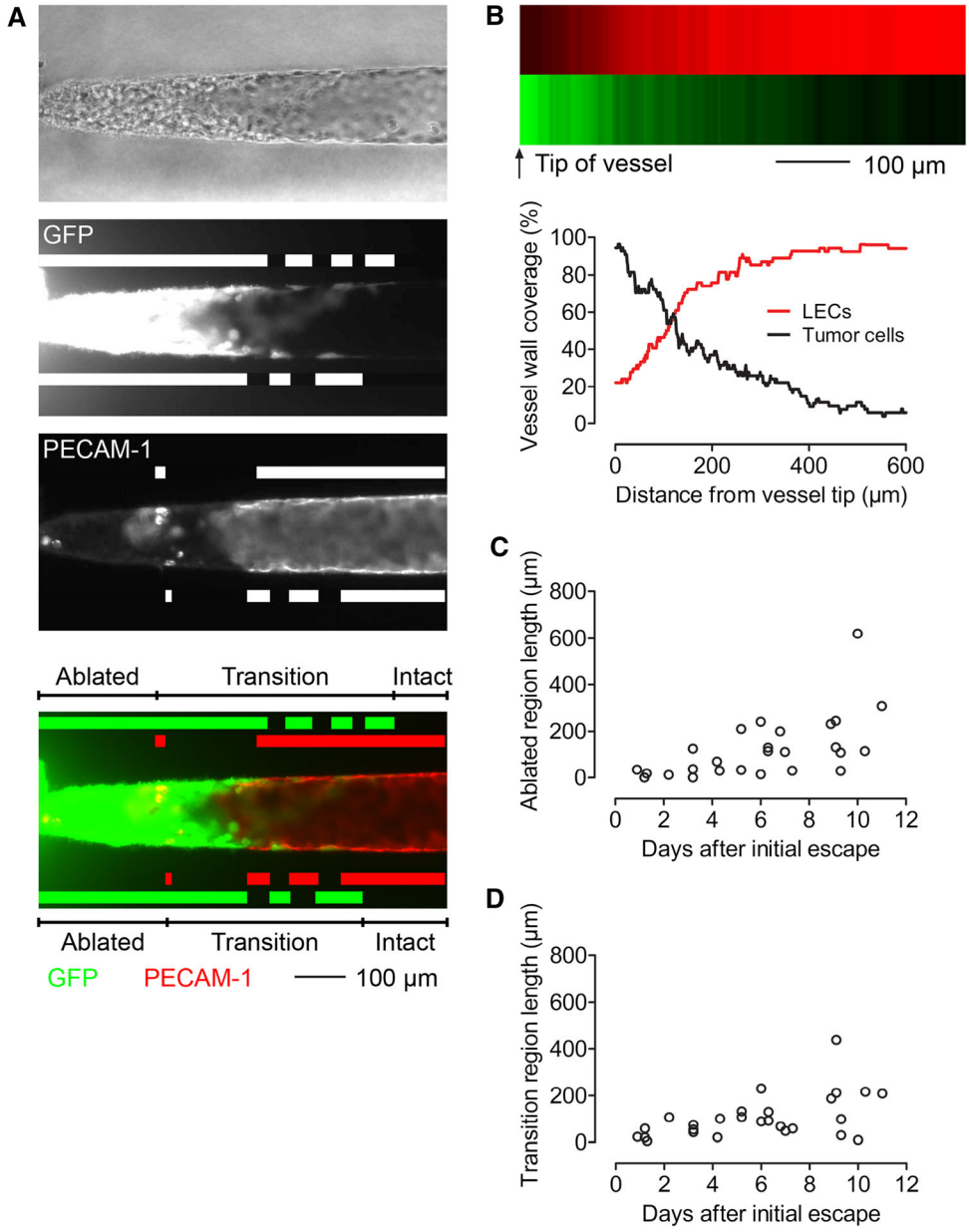

FIGURE 5. Ablation of lymphatic endothelium by escaped tumor cells. (A) Example of ablation analysis at day 16: (*top*) phase-contrast image of the midplane of the vessel, (*top-middle*) fluorescence image of GFP signal with binary maps of tumor coverage along vessel border, (*bottom-middle*) fluorescence image of PECAM-1 signal with binary maps of endothelial coverage along vessel border, (*bottom*) merged fluorescence image denoting ablated, transition, and intact regions of lymphatic vessel. (B) LEC and tumor cell coverage along vessels of escaped tumors at day 16: (*top*) heatmap and (*bottom*) corresponding plot of the percentage of the vessel wall lined by LECs or tumor cells within the first 600 μm of the vessel tip. (C) Length of ablated region of tumor-lymphatic samples versus time after escape. (D) Length of transition region of tumor-lymphatic samples versus time after escape. Data in (C) and (D) are from 27 tumors.

to lymphatic vessels grew more slowly than microtumors that were adjacent to empty cavities did ($p < 0.0001$; Fig. 7A). The shortest distance between any tumor cell and the cavity or lymphatic was measured daily and found to be larger for tumors adjacent to a lymphatic vessel than for tumors adjacent to an empty cavity on day 6 ($p < 0.05$), day 7 ($p < 0.01$), and day 8 ($p < 0.01$) (Fig. 7B). Microtumors approached empty cavities at a greater speed than they approached lymphatic vessels ($p < 0.0001$; Fig. 7C). In tumors that were adjacent to lymphatic vessels, we sometimes observed that tumor cells came into contact with the vessel one or more days before escape occurred (Fig. 3A). In tumors that were adjacent to empty cavities, however, cells were only rarely observed overlapping the cavity without having fully

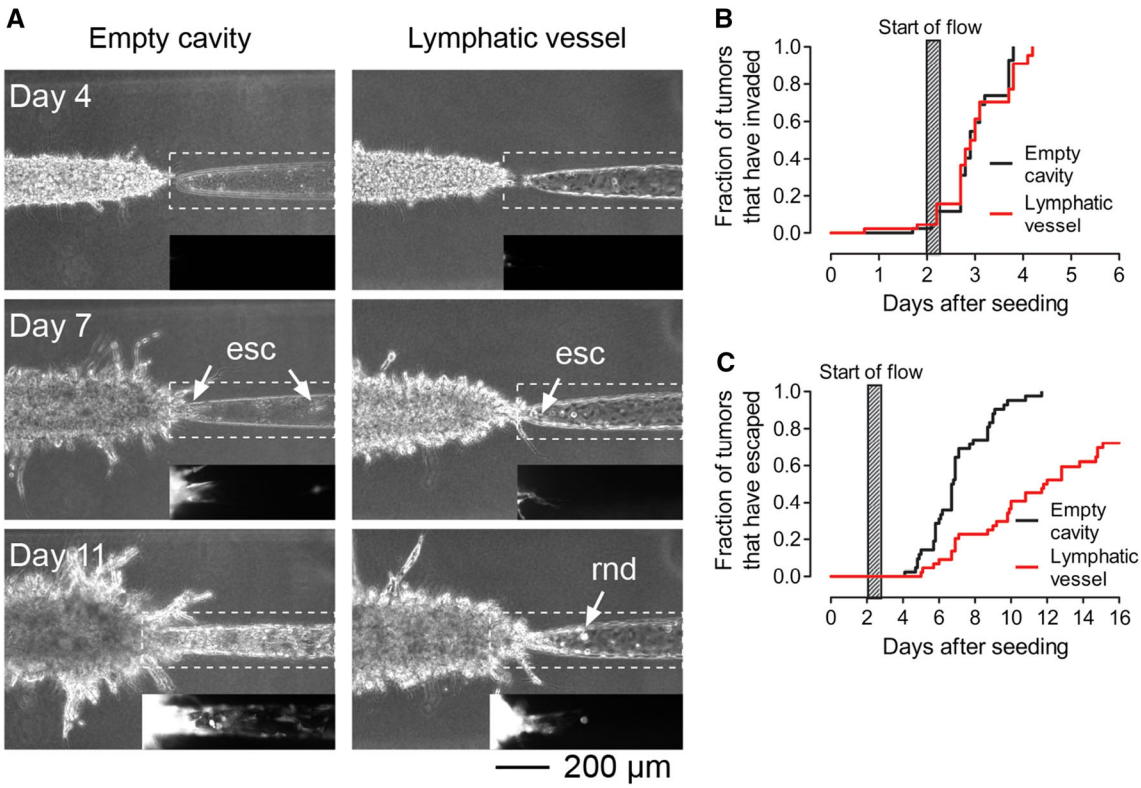

FIGURE 6. Lymphatic endothelium slows tumor cell escape. (A) Time-lapse images of microtumor progression into empty or LEC-lined cavities. *Insets*, fluorescence images of dashed regions. Arrows indicate escaped ("esc") and intravascular, rounded ("rnd") cancer cells. The tumor-lymphatic sample is the same one shown in Fig. 3B. (B) Kaplan–Meier plot of tumor invasion kinetics. (C) Kaplan–Meier plot of tumor escape kinetics. Data in (B) and (C) are from 42 tumor-cavity and 44 tumor-lymphatic samples.

escaped. We found that the lymphatic endothelium delayed tumor cell escape into the adjacent cavity ($p < 0.0001$; Fig. 7D). To further assess the progression of cancer cells along the cavity after escape, we measured the speed at which the tumor cells spread post-escape. The lymphatic endothelium slowed the spread of cancer cells along the cavity by a factor of ~ 4 ($p < 0.0001$; Fig. S3A). These data suggest that the presence of a lymphatic endothelium delays tumor cell escape at multiple stages.

LEC-Conditioned Medium Slows Tumor Escape

Since lymphatic vessels slowed the growth and movement of microtumors before tumor cells came into physical contact with endothelium, we reasoned that the LECs may be altering tumor behavior (including potentially the subsequent escape) through the release or consumption of soluble factors. To test this hypothesis, we fed distance-matched tumors (Fig. S2D) with either control medium or LEC-conditioned medium (CM) and monitored their invasion and escape into adjacent empty cavities (Fig. 8A). CM had no effect on the kinetics of initial invasion ($p = 0.91$; Fig. 8B). Tumors that were fed with CM escaped later than those that were fed with control medium did ($p < 0.0001$; *HR* 6.3; 95% CI 3.1–12.6; Fig. 8C).

We also measured other metrics of tumor advancement, including tumor growth rate, tumor speed toward the adjacent cavity, and speed of post-escape spread along the cavity. Microtumors that were fed with CM grew at a slower rate than microtumors that were fed with control medium did ($p < 0.0001$; Fig. 8D). The distance between the nearest tumor cell and the cavity was measured daily and found to be larger for tumors fed with CM than for tumors fed with control medium on day 4 ($p < 0.001$), day 5 ($p < 0.001$), day 6 ($p < 0.001$), and day 7 ($p < 0.01$) (Fig. 8E). Tumor speed toward the cavity was slower in tumors fed with CM than in tumors fed with control medium ($p < 0.0001$; Fig. 8F). In contrast, CM did not cause a delay in tumor cell escape after the cells had reached the adjacent cavity ($p = 0.29$; Fig. 8G). CM slowed the spread of tumor cells along the cavity post-escape by a factor of ~ 2 ($p < 0.0001$; Fig. S3B). Thus, treatment of tumors with lymphatic CM phenocopied nearly all of the effects of lymphatic endothelium in hindering escape. Given that lymphatic

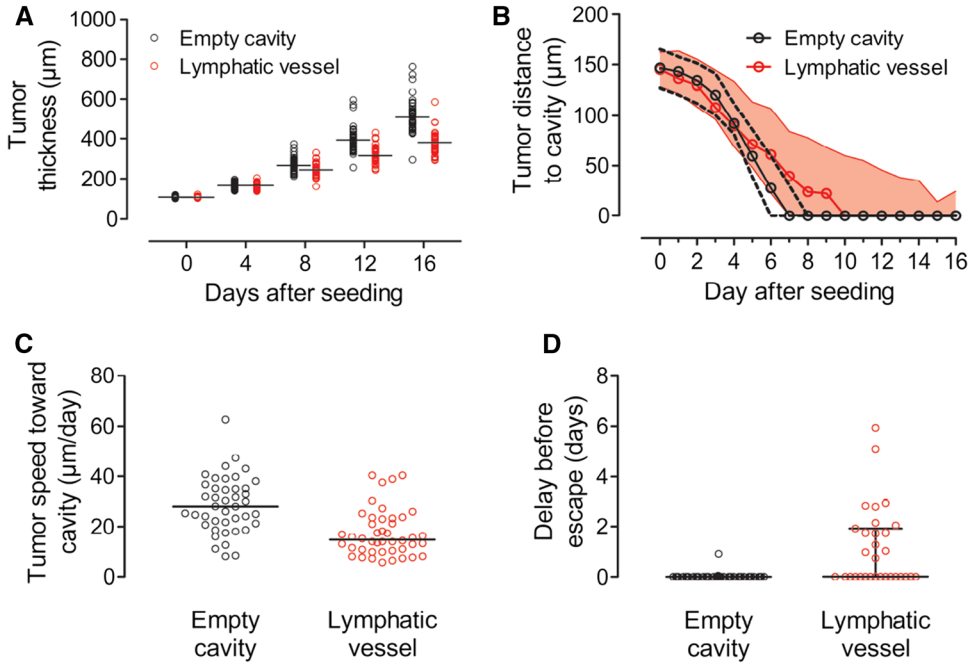

FIGURE 7. Effect of lymphatic endothelium on tumor progression. (A) Tumor growth over time. Bars indicate mean values. Data are from 42 tumor-cavity and 38 tumor-lymphatic samples. (B) Tumor-cavity distance over time. Black and red solid lines represent median values. Black dotted region and red shaded region both represent 25th and 75th percentiles. (C) Tumor speed toward cavity. Bars indicate median values. Data in (B) and (C) are from 42 tumor-cavity and 44 tumor-lymphatic samples. (D) Time of delay between when a tumor cell reaches the vessel or cavity and when it escapes. Bars indicate median values and interquartile ranges. Data are from 42 tumor-cavity and 31 tumor-lymphatic samples.

endothelium caused a delay in escape after the tumor cells reached the cavity, while lymphatic CM did not, the lymphatic endothelium likely acts as a physical barrier to escape as well.

DISCUSSION

In this study, we used a tissue-engineered human breast tumor model that contained blind-ended lymphatic vessels to reveal that the lymphatic endothelium slows tumor invasion, escape, and post-escape spread, and that these effects are largely reproduced when lymphatic-free tumors are treated with LEC-conditioned medium. Vessel-free tumor models have been used to evaluate the effects of interstitial fluid pressure, matrix pore size, matrix metalloproteinase activity, tumor cell proliferation, and adipose stroma on breast cancer cell invasion and escape into empty cavities.[11,39,46,47] The current study builds upon past models by adding LECs to line the cavity adjacent to the microtumor and transforming the cavity into a vessel that resembles a lymphatic capillary. We and others have engineered perfusable and blind-ended lymphatic tubes to model lymphatic vessels and demonstrated control over their barrier function in the absence or presence of tumor cells.[5,14,28,38,45]

Escape in Engineered Microvessels and Comparison with In Vivo Findings

Escaped tumor cells were located in several positions relative to the endothelium. First, and most commonly in samples that had escaped several days beforehand, tumor cells were found in regions devoid of endothelium. The length of these "ablated" regions correlated with time after escape, which implies that ablation is a continuous process that follows escape. Second, in regions that contained intact endothelium, tumor cells were detected in an intravascular location. We cannot formally ascribe this location to the presence of prior intravasation, although it is consistent with intravasation being a relatively early event in escape. Roughly 50% of tumors displayed this type of localization within five days of initial escape. Third, tumor cells were found in an extravascular location, nestled between the collagen and the endothelium.

Similar results have been reported for the escape of breast and other cancer cells into engineered blood microvessels.[34,43,51,52] Wong and Searson used time-lapse videos to record the intravasation of MDA-MB-231 breast cancer cells into engineered blood vessels.[51,52] Notably, they observed tumor cells spreading between the endothelium and the collagen wall in their microvessels. Silvestri *et al.* describe the *in vitro* formation of "mosaic" vessels in which the vessel wall is

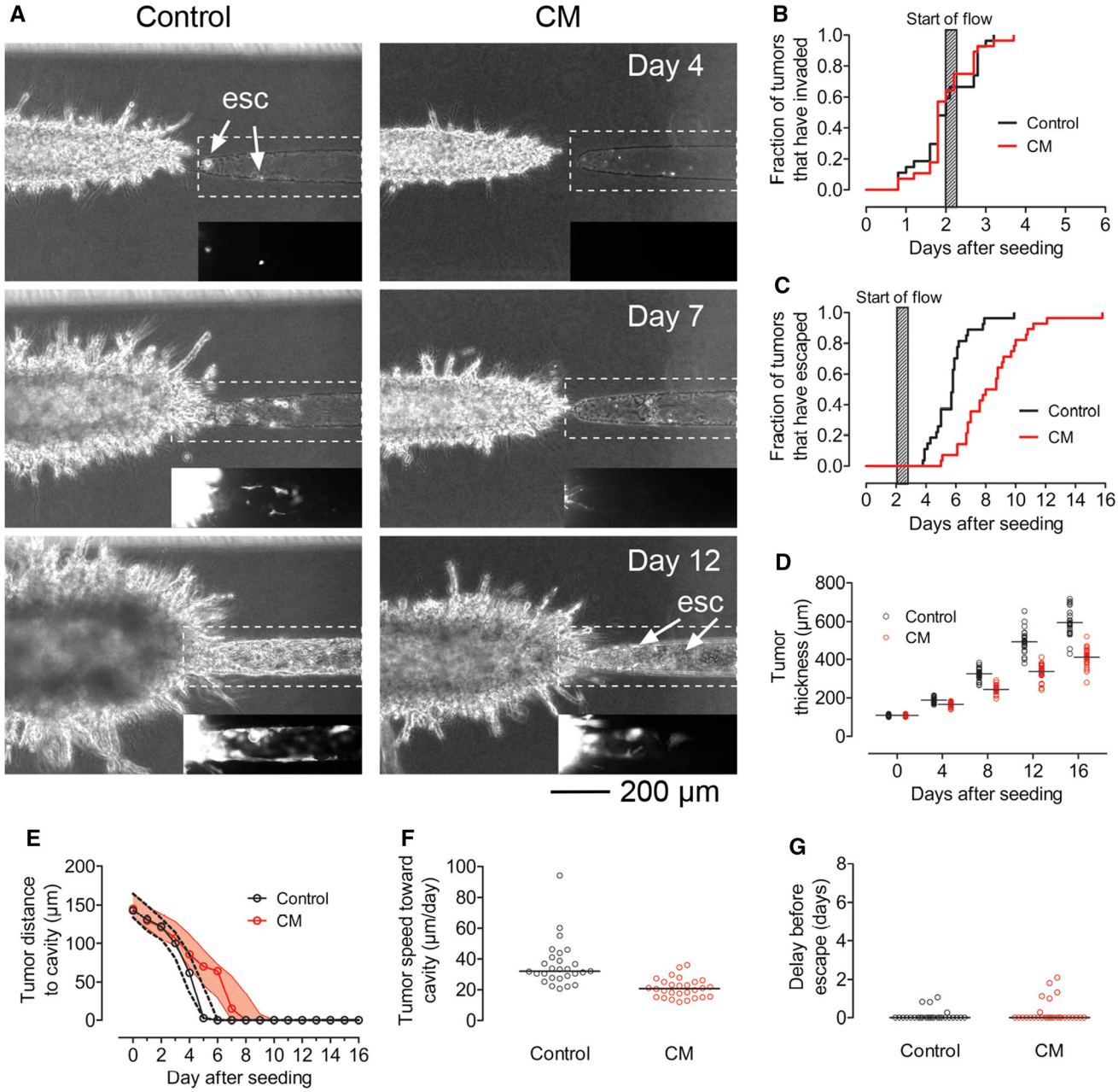

FIGURE 8. LEC-conditioned medium slows tumor escape into cavities. (A) Time-lapse images of microtumor progression for tumors fed with either control medium or LEC-conditioned medium (CM). *Insets*, fluorescence images of dashed regions. Arrows indicate escaped cancer cells (“esc”). (B-G) Metrics of tumor progression for tumors treated with control or CM. (B) Kaplan–Meier plot of tumor invasion kinetics. (C) Kaplan–Meier plot of tumor escape kinetics. (D) Tumor growth over time. Bars indicate mean values. (E) Tumor-cavity distance over time. Black and red solid lines represent median values. Black dotted region and red shaded region both represent 25th and 75th percentiles. (F) Tumor speed toward cavity. Bars indicate median values. (G) Time of delay between when a tumor cell reaches the cavity and when it escapes. Bars indicate median values and interquartile ranges. Data in (B)-(G) are from 27 control tumors and 28 tumors that were treated with CM.

lined by a mixture of tumor cells and endothelial cells.[43] That study also found mosaic vessels in human and murine breast tumors. Nguyen *et al.* found that pancreatic tumors ablate endothelium at the walls of engineered blood vessels.[34] Altogether, those studies and ours imply that breast cancer cells escape in the presence of blood and lymphatic vessels in qualitatively similar ways, although the quantitative kinetics depend on the context.

It is widely accepted that tumor cells can enter lymphatic vessels *in vivo via* intravasation, either by transmigrating through small intercellular gaps in the endothelium or by inducing larger holes in the endothelium to gain access to the lumen.[3] Histological

evidence of intravasation (also known as "lymphovascular invasion" or LVI) consists of the detection of tumor cells within a lymphatic lumen, similar to our intravascular detection of rounded, escaped tumor cells.[23,29] Examples of LVI in breast cancer include instances where clusters of invading cancer cells are found at discontinuities in the lymphatic endothelium, which is consistent with the ablation of endothelium by tumor cells that we observed in this study.[23,29] In contrast to these studies, we did not observe the complete filling of intact lymphatic lumens by tumor cell aggregates. This difference could arise from the short timescale of our experiments or the tendency for cancer cells in this model to spread extravascularly. Forms of extravascular tumor spread include angiotropism and vessel co-option, which are mainly observed in melanoma and glioblastoma, respectively.[24,27] The prevalence of extravascular spread of tumor cells and ablation of endothelium in engineered *in vitro* models, and the prevalence of intravasation of tumor cells *in vivo*, suggest that further optimization is needed for these models to more closely match the escape process described *in vivo*.

Histological studies have described the presence of vessel-like cavities without endothelial cells in the microenvironment surrounding breast tumors, referred to as "retraction artifacts" or "pre-lymphatics".[1,8,10] Acs *et al.* found retraction artifacts in 60% of tissue sections taken from patients with early-stage invasive breast carcinoma.[1] The presence of these cavities correlates with lymphatic vessel density, VEGF-C expression, LVI, and lymph node metastasis, and predicts poor prognosis in patients with early-stage breast cancer.[1,2] The presence of these endothelium-free cavities and their correlation with increased cancer spread support the importance of studying breast cancer escape into empty cavities. Our data also provide an alternate interpretation of tumor-filled cavities in histological sections, namely, that these features may be the result of sectioning a tumor where endothelial ablation has occurred. This interpretation would be consistent with the correlation between these histological features and LVI.

Role of Lymphatic Endothelium in Breast Tumor Invasion and Escape

Our results show that the presence of a lymphatic endothelium slows the escape of tumor cells. Similarly, escaped tumor cells migrate faster along empty cavities than along LEC-lined cavities. Addition of LEC-conditioned medium phenocopies the effect of lymphatic endothelium in almost all respects, which implies that LECs can affect tumor invasion and escape *via* chemical factors. This result contrasts with the finding that tumor-exposed LECs secrete more EGF than control LECs do, which boosts proliferation of MDA-MB-231 cells.[25] In addition, tumor cell-secreted VEGF-C can induce CCL21 release from LECs, which in turn can induce breast cancer cell chemotaxis through CCR7 signaling.[19,42] We found that lymphatic endothelium inhibits breast tumor invasion and escape despite vessels being in close proximity to the tumor cells. It is possible that the flow of medium toward the tumor in our system could decrease tumor-to-lymphatic signaling and hence limit the effect of the tumor on LEC gene expression. The use of conditioned medium from LECs that are co-cultured with tumor cells may help shed light on these differences.

Quiescent and activated/inflamed endothelium can have differing effects on tumor growth/proliferation. Franses *et al.* showed that conditioned medium from quiescent human umbilical vein endothelial cells (HUVECs) decreases proliferation in breast and lung cancer cells compared to fresh medium.[12] Silencing HUVEC expression of perlecan, a basement membrane-associated heparan sulfate proteoglycan, eliminated the inhibitory effect. Notably, LECs are known to express perlecan.[41] The LECs in our model proliferate very rarely (~ 1% EdU^+), which is a property of quiescent endothelium. In contrast, dysfunctional or activated endothelial cells promote tumor growth and metastasis by activating NF-κB and STAT3 in lung cancer cells.[13] Activation of endothelial NF-κB has been shown to promote the formation of 12(S)-HETE-induced defects in LEC monolayers by breast cancer cells and intravasation of breast cancer cells into lymphatic vessels.[33,48,50] Future work will investigate whether inflaming the lymphatic endothelium eliminates its ability to inhibit tumor cell escape or even promotes escape.

Limitations of the Breast Tumor/Lymphatic Model

An important limitation of the current model is the use of high intraluminal pressures and non-physiological flow direction from the lymphatic to the tumor. This flow condition was applied because 1) tumor cell invasion in these models currently requires flow toward the tumor[47] and 2) engineered lymphatic vessels have poor long-term stability when the interstitial pressure exceeds intraluminal pressure.[45] A more physiological flow condition will require the development of methods to stabilize lymphatics, such as by incorporating matrix components that strengthen endothelial adhesion to the cavity wall. A second limitation of the model is that the engineered lymphatics may be less permeable compared to lymphatic vessels *in vivo*. To promote lymphatic vessel stability, we supplemented sample medium with db-cAMP, which is known to

tighten endothelial junctions.[18] In principle, a tight endothelial barrier in these *in vitro* systems could favor ablation and tumor cell spread between the endothelium and collagen wall as opposed to tumor cell intravasation through gaps between adjacent endothelial cells. Third, most likely due to the presence of stabilizing culture conditions, the LECs rarely proliferated in this model. The low rate of proliferation contrasts with the hyperproliferative state often reported in tumor-associated lymphatics.[40] Fourth, since our findings are based purely on morphometric data, we lack any molecular details into how lymphatics hinder tumor progression. Fifth, the current study only formed tumors from the MDA-MB-231 triple-negative breast cancer cell line. The conclusions from this study cannot be generalized to tumors of other triple-negative breast cancer cells or to tumors of other molecular subtypes.

CONCLUSIONS

We have engineered an *in vitro* 3D model to study the escape of breast microtumors into LEC-lined cavities. In this model, tumor cells that escape into the LEC-lined cavity are found between the endothelium and the collagen wall, in line with the endothelium, or within the endothelial lumen. Over time, tumor cells replace the endothelium and create a region that is devoid of endothelium, starting from the tip of the lymphatic vessel. Lining cavities with lymphatic endothelium slows invasion speed and escape of breast microtumors into those cavities. Addition of LEC-conditioned medium is enough to slow invasion speed and escape of breast microtumors into empty cavities, which suggests an inhibitory role for LEC-conditioned medium in tumor invasion and escape. Developing engineered lymphatics that are stable when subjected to negative transmural pressure will allow a re-assessment of tumor-lymphatic interactions under more physiological flow conditions.

SUPPLEMENTARY INFORMATION

The online version contains supplementary material available at https://doi.org/10.1007/s12195-022-00745-9.

ACKNOWLEDGMENTS

We thank Xin Brown and Usman Ghani for assistance with experiments and Emily Margolis for helpful discussions. This study was funded by award U01 CA214292 from the National Cancer Institute. Y.W.D. was supported by a training grant from the National Institute of General Medical Sciences (award T32 GM008764) and by a fellowship from the CURE Diversity Research Supplements Program at the National Cancer Institute. O.M.K. was funded by the Undergraduate Research Opportunities Program at Boston University.

CONFLICT OF INTEREST

Alex J. Seibel, Owen M. Kelly, Yoseph W. Dance, Celeste M. Nelson, and Joe Tien declare that they have no conflict of interest.

ETHICAL APPROVAL

No human or animal studies were carried out by the authors for this article.

REFERENCES

[1]Acs, G., K. L. Dumoff, L. J. Solin, T. Pasha, X. Xu, and P. J. Zhang. Extensive retraction artifact correlates with lymphatic invasion and nodal metastasis and predicts poor outcome in early stage breast carcinoma. *Am. J. Surg. Pathol.* 31:129–140, 2007.

[2]Acs, G., G. Paragh, Z. Rakosy, C. Laronga, and P. J. Zhang. The extent of retraction clefts correlates with lymphatic vessel density and VEGF-C expression and predicts nodal metastasis and poor prognosis in early-stage breast carcinoma. *Mod. Pathol.* 25:163–177, 2012.

[3]Alitalo, A., and M. Detmar. Interaction of tumor cells and lymphatic vessels in cancer progression. *Oncogene* 31:4499–4508, 2012.

[4]Andersson, Y., L. Bergkvist, J. Frisell, and J. de Boniface. Long-term breast cancer survival in relation to the metastatic tumor burden in axillary lymph nodes. *Breast Cancer Res. Treat.* 171:359–369, 2018.

[5]Ayuso, J. M., M. M. Gong, M. C. Skala, P. M. Harari, and D. J. Beebe. Human tumor-lymphatic microfluidic model reveals differential conditioning of lymphatic vessels by breast cancer cells. *Adv. Healthc. Mater.* 9:1900925, 2020.

[6]Breslin, J. W., Y. Yang, J. P. Scallan, R. S. Sweat, S. P. Adderley, and W. L. Murfee. Lymphatic vessel network structure and physiology. *Compr. Physiol.* 9:207–299, 2018.

[7]Cabioglu, N., M. S. Yazici, B. Arun, K. R. Broglio, G. N. Hortobagyi, J. E. Price, and A. Sahin. CCR7 and CXCR4 as novel biomarkers predicting axillary lymph node metastasis in T_1 breast cancer. *Clin. Cancer Res.* 11:5686–5693, 2005.

[8]Casley-Smith, J. R. 'Prelymphatic': a question of terminology? *Experientia* 38:1123–1124, 1982.

[9]Dadiani, M., V. Kalchenko, A. Yosepovich, R. Margalit, Y. Hassid, H. Degani, and D. Seger. Real-time imaging of lymphogenic metastasis in orthotopic human breast cancer. *Cancer Res.* 66:8037–8041, 2006.

[10]Damiani, S., J. L. Peterse, and V. Eusebi. Malignant neoplasms infiltrating 'pseudoangiomatous' stromal hyperplasia of the breast: an unrecognized pathway of tumour spread. *Histopathology* 41:208–215, 2002.
[11]Dance, Y. W., T. Meshulam, A. J. Seibel, M. C. Obenreder, M. D. Layne, C. M. Nelson, and J. Tien. Adipose stroma accelerates the invasion and escape of human breast cancer cells from an engineered microtumor. *Cell. Mol. Bioeng.* 15:15–29, 2022.
[12]Franses, J. W., A. B. Baker, V. C. Chitalia, and E. R. Edelman. Stromal endothelial cells directly influence cancer progression. *Sci. Transl. Med.* 3:66ra5, 2011.
[13]Franses, J. W., N. C. Drosu, W. J. Gibson, V. C. Chitalia, and E. R. Edelman. Dysfunctional endothelial cells directly stimulate cancer inflammation and metastasis. *Int. J. Cancer* 133:1334–1344, 2013.
[14]Gong, M. M., K. M. Lugo-Cintron, B. R. White, S. C. Kerr, P. M. Harari, and D. J. Beebe. Human organotypic lymphatic vessel model elucidates microenvironment-dependent signaling and barrier function. *Biomaterials* 214:119225, 2019.
[15]Greenlee, J. D., and M. R. King. Engineered fluidic systems to understand lymphatic cancer metastasis. *Biomicrofluidics* 14:011502, 2020.
[16]Hasselhof, V., A. Sperling, K. Buttler, P. Ströbel, J. Becker, T. Aung, G. Felmerer, and J. Wilting. Morphological and molecular characterization of human dermal lymphatic collectors. *PLoS One* 11:e0164964, 2016.
[17]Hayashi, K., P. Jiang, K. Yamauchi, N. Yamamoto, H. Tsuchiya, K. Tomita, A. R. Moossa, M. Bouvet, and R. M. Hoffman. Real-time imaging of tumor-cell shedding and trafficking in lymphatic channels. *Cancer Res.* 67:8223–8228, 2007.
[18]He, P., M. Zeng, and F. E. Curry. Dominant role of cAMP in regulation of microvessel permeability. *Am. J. Physiol. Heart Circ. Physiol.* 278:H1124–H1133, 2000.
[19]Issa, A., T. X. Le, A. N. Shoushtari, J. D. Shields, and M. A. Swartz. Vascular endothelial growth factor-C and C-C chemokine receptor 7 in tumor cell–lymphatic cross-talk promote invasive phenotype. *Cancer Res.* 69:349–357, 2009.
[20]Jatoi, I., S. G. Hilsenbeck, G. M. Clark, and C. K. Osborne. Significance of axillary lymph node metastasis in primary breast cancer. *J. Clin. Oncol.* 17:2334–2340, 1999.
[21]Karaman, S., and M. Detmar. Mechanisms of lymphatic metastasis. *J. Clin. Invest.* 124:922–928, 2014.
[22]Kedrin, D., B. Gligorijevic, J. Wyckoff, V. V. Verkhusha, J. Condeelis, J. E. Segall, and J. van Rheenen. Intravital imaging of metastatic behavior through a mammary imaging window. *Nat. Methods* 5:1019–1021, 2008.
[23]Kerjaschki, D., Z. Bago-Horvath, M. Rudas, V. Sexl, C. Schneckenleithner, S. Wolbank, G. Bartel, S. Krieger, R. Kalt, B. Hantusch, T. Keller, K. Nagy-Bojarszky, N. Huttary, I. Raab, K. Lackner, K. Krautgasser, H. Schachner, K. Kaserer, S. Rezar, S. Madlener, C. Vonach, A. Davidovits, H. Nosaka, M. Hämmerle, K. Viola, H. Dolznig, M. Schreiber, A. Nader, W. Mikulits, M. Gnant, S. Hirakawa, M. Detmar, K. Alitalo, S. Nijman, F. Offner, T. J. Maier, D. Steinhilber, and G. Krupitza. Lipoxygenase mediates invasion of intrametastatic lymphatic vessels and propagates lymph node metastasis of human mammary carcinoma xenografts in mouse. *J. Clin. Invest.* 121:2000–2012, 2011.
[24]Kuczynski, E. A., and A. R. Reynolds. Vessel co-option and resistance to anti-angiogenic therapy. *Angiogenesis* 23:55–74, 2020.
[25]Lee, E., N. B. Pandey, and A. S. Popel. Lymphatic endothelial cells support tumor growth in breast cancer. *Sci. Rep.* 4:5853, 2014.
[26]Leung, A. D., K. H. K. Wong, and J. Tien. Plasma expanders stabilize human microvessels in microfluidic scaffolds. *J. Biomed. Mater. Res. A* 100:1815–1822, 2012.
[27]Lugassy, C., H. K. Kleinman, P. B. Vermeulen, and R. L. Barnhill. Angiotropism, pericytic mimicry and extravascular migratory metastasis: an embryogenesis-derived program of tumor spread. *Angiogenesis* 23:27–41, 2020.
[28]Lugo-Cintrón, K. M., J. M. Ayuso, B. R. White, P. M. Harari, S. M. Ponik, D. J. Beebe, M. M. Gong, and M. Virumbrales-Muñoz. Matrix density drives 3D organotypic lymphatic vessel activation in a microfluidic model of the breast tumor microenvironment. *Lab Chip* 20:1586–1600, 2020.
[29]Mohammed, R. A. A., S. G. Martin, M. S. Gill, A. R. Green, E. C. Paish, and I. O. Ellis. Improved methods of detection of lymphovascular invasion demonstrate that it is the predominant method of vascular invasion in breast cancer and has important clinical consequences. *Am. J. Surg. Pathol.* 31:1825–1833, 2007.
[30]Nathanson, S. D., D. Kwon, A. Kapke, S. H. Alford, and D. Chitale. The role of lymph node metastasis in the systemic dissemination of breast cancer. *Ann. Surg. Oncol.* 16:3396–3405, 2009.
[31]Nathanson, S. D., S. Leonard-Murali, C. Burmeister, L. Susick, and P. Baker. Clinicopathological evaluation of the potential anatomic pathways of systemic metastasis from primary breast cancer suggests an orderly spread through the regional lymph nodes. *Ann. Surg. Oncol.* 27:4810–4818, 2020.
[32]Nathanson, S. D., M. Detmar, T. P. Padera, L. R. Yates, D. R. Welch, T. C. Beadnell, A. D. Scheid, E. D. Wrenn, and K. Cheung. Mechanisms of breast cancer metastasis. *Clin. Exp. Metastasis* 39:117–137, 2022.
[33]Nguyen, C. H., D. Senfter, J. Basilio, S. Holzner, S. Stadler, S. Krieger, N. Huttary, D. Milovanovic, K. Viola, I. Simonitsch-Klupp, W. Jäger, R. de Martin, and G. Krupitza. NF-κB contributes to MMP1 expression in breast cancer spheroids causing paracrine PAR1 activation and disintegrations in the lymph endothelial barrier in vitro. *Oncotarget* 6:39262–39275, 2015.
[34]Nguyen, D.-H.T., E. Lee, S. Alimperti, R. J. Norgard, A. Wong, J.J.-K. Lee, J. Eyckmans, B. Z. Stanger, and C. S. Chen. A biomimetic pancreatic cancer on-chip reveals endothelial ablation via ALK7 signaling. *Sci. Adv.* 5:eaav6789, 2019.
[35]Pereira, E. R., D. Kedrin, G. Seano, O. Gautier, E. F. J. Meijer, D. Jones, S.-M. Chin, S. Kitahara, E. M. Bouta, J. Chang, E. Beech, H.-S. Jeong, M. C. Carroll, A. G. Taghian, and T. P. Padera. Lymph node metastases can invade local blood vessels, exit the node, and colonize distant organs in mice. *Science* 359:1403–1407, 2018.
[36]Piotrowski-Daspit, A. S., A. K. Simi, M.-F. Pang, J. Tien, and C. M. Nelson. A 3D culture model to study how fluid pressure and flow affect the behavior of aggregates of epithelial cells. In: Mammary Gland Development, edited by F. Martin, T. Stein, and J. Howlin. New York: Springer, 2017, pp. 245–257.
[37]Pisano, M., V. Triacca, K. A. Barbee, and M. A. Swartz. An in vitro model of the tumor-lymphatic microenviron-

ment with simultaneous transendothelial and luminal flows reveals mechanisms of flow enhanced invasion. *Integr. Biol.* 7:525–533, 2015.
[38]Price, G. M., K. M. Chrobak, and J. Tien. Effect of cyclic AMP on barrier function of human lymphatic microvascular tubes. *Microvasc. Res.* 76:46–51, 2008.
[39]Rabie, E. M., S. X. Zhang, A. P. Kourouklis, A. N. Kilinc, A. K. Simi, D. C. Radisky, J. Tien, and C. M. Nelson. Matrix degradation and cell proliferation are coupled to promote invasion and escape from an engineered human breast microtumor. *Integr. Biol.* 13:17–29, 2021.
[40]Ran, S., L. Volk, K. Hall, and M. J. Flister. Lymphangiogenesis and lymphatic metastasis in breast cancer. *Pathophysiology* 17:229–251, 2010.
[41]Rutkowski, J. M., K. C. Boardman, and M. A. Swartz. Characterization of lymphangiogenesis in a model of adult skin regeneration. *Am. J. Physiol. Heart Circ. Physiol.* 291:H1402–H1410, 2006.
[42]Shields, J. D., M. E. Fleury, C. Yong, A. A. Tomei, G. J. Randolph, and M. A. Swartz. Autologous chemotaxis as a mechanism of tumor cell homing to lymphatics via interstitial flow and autocrine CCR7 signaling. *Cancer Cell* 11:526–538, 2007.
[43]Silvestri, V. L., E. Henriet, R. M. Linville, A. D. Wong, P. C. Searson, and A. J. Ewald. A tissue-engineered 3D microvessel model reveals the dynamics of mosaic vessel formation in breast cancer. *Cancer Res.* 80:4288–4301, 2020.
[44]Steeg, P. S. Tumor metastasis: mechanistic insights and clinical challenges. *Nat. Med.* 12:895–904, 2006.
[45]Thompson, R. L., E. A. Margolis, T. J. Ryan, B. J. Coisman, G. M. Price, K. H. K. Wong, and J. Tien. Design principles for lymphatic drainage of fluid and solutes from collagen scaffolds. *J. Biomed. Mater. Res. A* 106:106–114, 2018.
[46]Tien, J., Y. W. Dance, U. Ghani, A. J. Seibel, and C. M. Nelson. Interstitial hypertension suppresses escape of human breast tumor cells via convection of interstitial fluid. *Cell. Mol. Bioeng.* 14:147–159, 2021.
[47]Tien, J., U. Ghani, Y. W. Dance, A. J. Seibel, M. Ç. Karakan, K. L. Ekinci, and C. M. Nelson. Matrix pore size governs escape of human breast cancer cells from a microtumor to an empty cavity. *iScience* 23:101673, 2020.
[48]Viola, K., S. Kopf, N. Huttary, C. Vonach, N. Kretschy, M. Teichmann, B. Giessrigl, I. Raab, S. Stary, S. Krieger, T. Keller, S. Bauer, B. Hantusch, T. Szekeres, R. de Martin, W. Jäger, W. Mikulits, H. Dolznig, G. Krupitza, and M. Grusch. Bay11-7082 inhibits the disintegration of the lymphendothelial barrier triggered by MCF-7 breast cancer spheroids; the role of ICAM-1 and adhesion. *Br. J. Cancer* 108:564–569, 2013.
[49]Visser, T. D., J. L. Oud, and G. J. Brakenhoff. Refractive index and axial distance measurements in 3-D microscopy. *Optik* 90:17–19, 1992.
[50]Vonach, C., K. Viola, B. Giessrigl, N. Huttary, I. Raab, R. Kalt, S. Krieger, T. P. N. Vo, S. Madlener, S. Bauer, B. Marian, M. Hämmerle, N. Kretschy, M. Teichmann, B. Hantusch, S. Stary, C. Unger, M. Seelinger, A. Eger, R. Mader, W. Jäger, W. Schmidt, M. Grusch, H. Dolznig, W. Mikulits, and G. Krupitza. NF-κB mediates the 12(S)-HETE-induced endothelial to mesenchymal transition of lymphendothelial cells during the intravasation of breast carcinoma cells. *Br. J. Cancer* 105:263–271, 2011.
[51]Wong, A. D., and P. C. Searson. Live-cell imaging of invasion and intravasation in an artificial microvessel platform. *Cancer Res.* 74:4937–4945, 2014.
[52]Wong, A. D., and P. C. Searson. Mitosis-mediated intravasation in a tissue-engineered tumor-microvessel platform. *Cancer Res.* 77:6453–6461, 2017.
[53]Wong, K. H. K., J. G. Truslow, and J. Tien. The role of cyclic AMP in normalizing the function of engineered human blood microvessels in microfluidic collagen gels. *Biomaterials* 31:4706–4714, 2010.
[54]Wu, S.-G., H. Li, L.-Y. Tang, J.-Y. Sun, W.-W. Zhang, F.-Y. Li, Y.-X. Chen, and Z.-Y. He. The effect of distant metastases sites on survival in de novo stage-IV breast cancer: a SEER database analysis. *Tumor Biol.* 39:1010428317705082, 2017.
[55]Wyckoff, J. B., Y. Wang, E. Y. Lin, J.-F. Li, S. Goswami, E. R. Stanley, J. E. Segall, J. W. Pollard, and J. Condeelis. Direct visualization of macrophage-assisted tumor cell intravasation in mammary tumors. *Cancer Res.* 67:2649–2656, 2007.
[56]Zhang, S., D. Zhang, S. Yi, M. Gong, C. Lu, Y. Cai, X. Tang, and L. Zou. The relationship of lymphatic vessel density, lymphovascular invasion, and lymph node metastasis in breast cancer: a systematic review and meta-analysis. *Oncotarget* 8:2863–2873, 2016.
[57]Zhang, S., D. Zhang, M. Gong, L. Wen, C. Liao, and L. Zou. High lymphatic vessel density and presence of lymphovascular invasion both predict poor prognosis in breast cancer. *BMC Cancer* 17:335, 2017.

Supplementary Figure 1: Images of negative controls acquired at exposure times matched to each immunofluorescence stain shown in **Fig. 2**. (A-D) Concentration-matched mouse IgG controls for (A) cytokeratin, (B) vimentin, (C) PECAM-1, and (D) VE-cadherin. Images were obtained from day 7 samples. Scale bars indicate 100 μm. (E) Prox1 (red) and Hoechst (blue) stain of tumor cells and LECs on coverslips. Scale bars indicate 50 μm.

Supplementary Figure 2: Matching of tumor-cavity and tumor-vessel samples by initial separation distances and flow rates over time. (A) Cumulative frequency distributions of initial tumor-cavity distances for tumors shown in **Figs. 6-7**. Data are from 42 tumor-cavity and 44 tumor-lymphatic samples. (B) Average flow rates measured over 12-16 hr for tumors shown in **Figs. 6-7**. (C) Applied pressure differences for tumors shown in **Figs. 6-7**. For plots in (B) and (C), black and red solid lines represent median values, and the black dotted region and red shaded region both represent 25th and 75th percentiles. Data in (B) and (C) are from 42 tumor-cavity and 38 tumor-lymphatic samples. (D) Cumulative frequency distributions of initial tumor-cavity distances for tumors shown in **Fig. 8**. CM, conditioned medium. Data are from 27 control tumors and 28 tumors treated with CM.

Supplementary Figure 3: Speed of distal spread for tumor cells after escape, for (A) tumors shown in **Figs. 6-7** and (B) tumors shown in **Fig. 8**. Bars indicate median values. CM, conditioned medium. Data in (A) are from 42 tumor-cavity and 31 tumor-lymphatic samples. Data in (B) are from 27 control tumors and 27 tumors treated with CM.

Supplementary Figure 1:

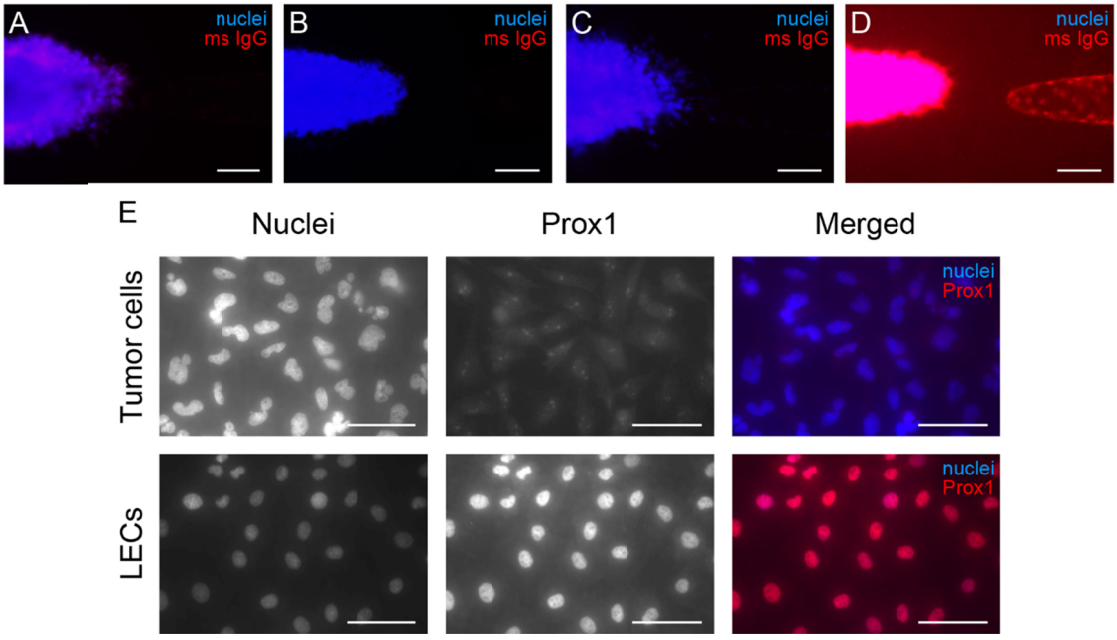

Supplementary Figure 2:

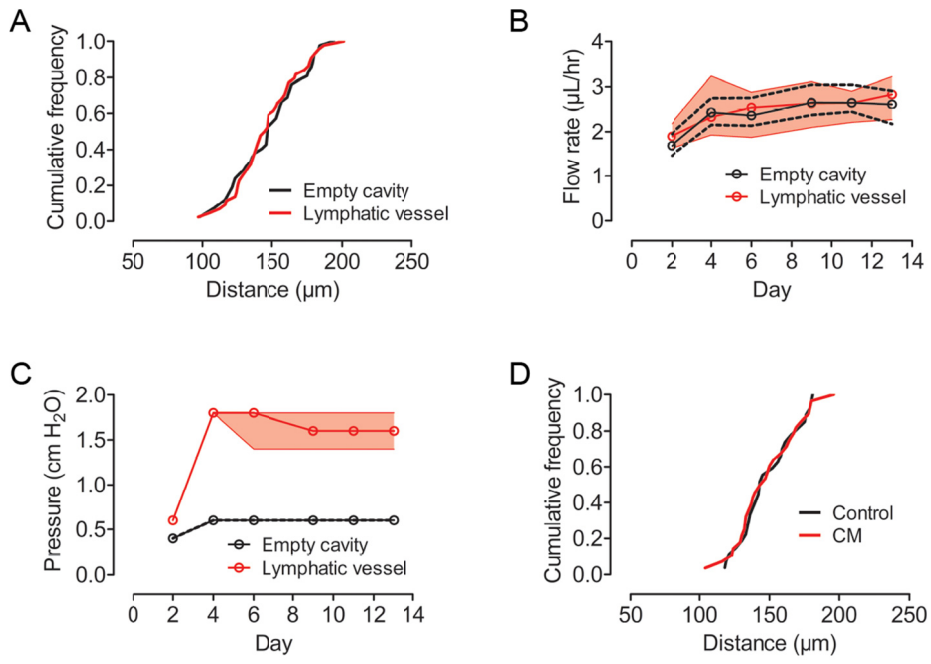

Supplementary Figure 3: